Published by IOP Publishing for Sissa Medialab

Received: *February 6, 2024*
Accepted: *August 27, 2024*
Published: *November 15, 2024*

Predominantly electric storage ring with nuclear spin control capability

Richard Talman[a] **and John Talman**[b]

[a] *Laboratory for Elementary-Particle Physics, Cornell University, Ithaca, NY, U.S.A.*
[b] *UAL Consultants, Ithaca, NY, U.S.A.*

E-mail: richard.talman@cornell.edu

Abstract: A predominantly electric E&m storage ring, with weak superimposed magnetic bending, is shown to be capable of storing two different particle type bunches, such as helion (h) and deuteron (d), or h and electron (e^-), co-traveling with different velocities on the same central orbit. Rear-end collisions occurring periodically in a full acceptance particle detector/polarimeter, allow the (previously inaccessible) direct measurement of the spin dependence of nuclear transmutation for center of mass (CM) kinetic energies (KE) ranging from hundreds of keV up toward pion production thresholds. With the nuclear process occurring in a semi-relativistic moving frame, all initial and final state particles have convenient laboratory frame KEs in the tens to hundreds of MeV. The rear-end collisions occur as faster stored bunches pass through slower bunches. An inexpensive facility capable of meeting these requirements is described, with several nuclear channels as examples. Especially noteworthy are the $e^{+/-}$-induced weak interaction triton (t) β-decay processes, $\mathrm{t} + e^+ \rightarrow \mathrm{h} + \nu$ and $\mathrm{h} + e^- \rightarrow \mathrm{t} + \nu$. Experimental capability of measurement of the spin dependence of the induced triton case is emphasized. For cosmological nuclear physics, the experimental improvement will be produced by the storage ring's capability to investigate the spin dependence of nuclear transmutation processes at reduced kinetic energies compared to what can be obtained with fixed target geometry.

Keywords: Accelerator Applications; Accelerator modelling and simulations (multi-particle dynamics, single-particle dynamics); Instrumentation for particle accelerators and storage rings - low energy (linear accelerators, cyclotrons, electrostatic accelerators); Low-energy ion storage

https://doi.org/10.1088/1748-0221/19/11/P11017

2024 JINST 19 P11017

Contents

1 Introduction

The proton is the only stable elementary particle for which no experimentally testable fundamental theory predictions exist! Direct p, p and p, n coupling is too strong for their interactions to be calculable using relativistic quantum field theory. Next-best: the meson-nucleon perturbation parameter (roughly 1/5) is small enough for standard model theory, with its quarks and gluons, to be based, numerically, predominantly on π meson, nucleon scattering. This *finesses* complications associated with finite size, internal structure, and compound nucleus formation.

These issues should be addressed experimentally, but this is seriously impeded by the absence of nuclear physics measurement, especially concerning spin dependence, for particle kinetic energies (KE) in the range from 100 keV to several MeV, comparable with Coulomb potential barrier heights. Even though multi-keV scale energies are easily produced in vacuum, until now spin measurement in

2024 JINST 19 P11017

this region has been prevented by space charge and negligibly short particle ranges in matter. In this energy range, negligible compared to all nucleon rest masses, the lab frame and the CM frame coincide.

To study spin dependence in nuclear scattering, one must cause the scattering to occur in what is (at least a weakly relativistic) moving frame of reference. This is possible using "rear-end" collisions in a predominantly electric E&m storage ring. Superimposed weak magnetic bending makes it possible for two beams of different velocity to circulate in the same direction, at the same time, in the same storage ring. "Rear-end" collisions occurring during the passage of faster bunches through slower bunches can be used to study spin dependence on nucleon-nucleon collisions in a moving coordinate frame.

Such "rear-end" collisions allow the CM KEs to be in the several 100 keV range, while all incident and scattered particles have convenient laboratory KEs, two orders of magnitude higher, in the tens of MeV range. Multi-MeV scale incident beams can then be established in pure spin states and the momenta and polarizations of all final state particles can be measured with high analyzing power and high efficiency. In this way the storage ring satisfies the condition that all nuclear collisions take place in a coordinate frame moving at convenient semi-relativistic speed in the laboratory, with CM KEs comparable with Coulomb barrier heights.

2 Importance of anomalous nuclear MDM G-values

One motivation for the E&m storage ring being promoted in this paper centers on the careful study of elastic or weakly inelastic nucleon scattering, and emphasizes the possible role played by the anomalous MDM, G. An essential feature of the rings being advocated here follows from their superimposed electric and magnetic bending, which provides the capability of simultaneously co- or counter-circulating frozen or pseudo-frozen spin beams of different particle type.

The original motivation for the development of E&m rings was to investigate time reversal violation in the form of non-vanishing proton electric dipole moment (EDM), which has always been assumed to constrain the strong nuclear force. But, in actuality, the electromagnetic and nuclear forces are inextricably connected in actual protons. The influence of this marriage has been well accounted for, in both classical and quantum mechanics, for low energy Rutherford scattering differential scattering cross sections. However, in p,p scattering, there is also proton spin precession caused by the (relativistically-implied) $\mathbf{B} = \mathbf{v} \times \mathbf{E}$ magnetic field (in the proton's rest frame) acting on the proton's anomalous magnetic moment [1] .

Appendix E of reference [3] discusses the consistent treatment of g-factor g and anomalous magnetic moment factor G and the conversion of g to G, following the treatment in reference [2], which explains how E&m storage rings can be utilized as "MDM Comparators". In the present context, when ultrahigh frequency domain MDM precision is required, it is appropriate to have runs long enough for spin orientations to complete an integral number of rotations after an integral number of turns. For this purpose it is appropriate to express the anomalous MDM as a rational fraction, in order to determine the minimum number of turns required, and the exact number of turns required to produce an integral number of spin revolutions. This capability is abbreviated to the phrase *with frequency domain precision* in the sequel.

The E&m storage ring configuration is ideal for the precision measurement of anomalous nuclear MDM G-values. Such rings serve naturally for the function of "mutual co-magnetometry" for precision experimental determination of G-values of nuclear particles.

2024 JINST 19 P11017

In the present context there is an equally important need for knowing the MDMs of nuclear isotopes to the highest possible precision. What needs to be explained is the way that storage ring steering can be set and reset to *frequency domain precision* (i.e. with precision that would be unachievable by direct field strength control) using the particle anomalous magnetic moments as "magnetometric gyroscopes".

For historical reasons, based probably on the great importance and successful application of the g-factor in atomic physics, the anomalous MDM parameter G, a fundamental measurable ratio of nucleus angular momentum (proportional to inertial mass m of nucleon) to magnetic moment (proportional to charge of the same nucleus) is less systematically updated and made available than is g. With Z and A being dimensionless measures, the ratio of integers, A/Z, justifies regarding $g(A/Z)$ as being a function of A and Z only via the ratio A/Z. To be "anomalous" the dimensionality of G and g must be the same: i.e. their ratio is dimensionless. For every nucleon, Z is truly an integer multiple of (positive) proton charge e. Regrettably, for example because of nuclear binding energy, nucleon mass ratios are only approximately given by the mass number A.

Precision storage rimg measurement of anomalous magnetic moments using storage rings with superimposed bending was first discussed in reference [2]. Further discussion is relegated to appendix E of reference [3], but not because it is unimportant. The present paper provides further strong support for the precise measurement, and consistent treatment of nuclear isotope MDMs and mass values. But the discussion is both detailed and technical. This justifies referring to that reference for discussion of the experimental and theoretical connections between g-factor and anomalous magnetic moment G [4–6]. Especially important is figure 35 at the end of reference [3], which, for many low mass isotopes, expresses G as the (dimensionless) rational fraction appropriate for its precise expression.

3 Superimposed E/B storage ring bending

This section, concerning the simultaneous storage of two different particle type beams in the circular arcs of a predominantly electric "E&m" storage ring with superimposed magnetic bending, is supposed to be clear on its own. To the extent this is not the case, it may be helpful to refer to appendix F, "Superimposed E&M storage rings" in reference [7].

For simplicity the arcs are assumed to be perfect circles, of bending radius r_0, joined tangentially by bend-free straight sections of arbitrary length. Without essential loss of generality, we assume the geometry has super-periodicity four, giving it the shape of a rounded square, or a squared-off circle.

Fractional bending coefficients η_E and η_m are defined by

$$\eta_E = \frac{qr_0}{pc/e}\,\frac{E_0}{\beta},\ \eta_M = \frac{qr_0}{pc/e}\,cB_0, \tag{3.1}$$

neither of which is necessarily positive.[1]

These fractional bending fractions satisfy

$$\eta_E + \eta_M = 1, \quad \text{and} \quad \frac{\eta_E}{\eta_M} = \frac{E_0/\beta}{cB_0}. \tag{3.2}$$

By symmetry, stable *all-electric* storage ring orbits are forward/backward symmetric and there are continua of different orbit velocities and radii, one of which matches the design ring radius r_0 in

[1]The discussion in this secction amounts to the introduction of "electric rigidity" to go along with, more familiar, magnetic rigidity. These quantities are proportional to the inverses of the coefficients in eqs. 3.1. For brevity, and to avoid unit-dependent confusion, the term "rigidities" will be used without formal definition in the sequal.

2024 JINST 19 P11017

each direction. To represent the required bending force at radius r_0 being augmented by magnetic bending while preserving the orbit curvature we require

$$\eta_E + \eta_M = 1, \tag{3.3}$$

where, typically, in the present paper, $|\eta_M| < |\eta_E|$. The resulting magnetic force dependence on direction causes an $\eta_M > 0$ (call this "constructive") or $\eta_M < 0$ ("destructive") perturbation to shift opposite direction orbit velocities (v) of the same radius, one up in radius and one down, resulting in two stable orbits in each direction. For stored beams, any further $\Delta\eta_M \neq 0$ change causes beam velocities to ramp up in kinetic energy ($KE = \mathcal{E} - mc^2$) in one direction, down in the other.

Our proposed E&m storage ring is ideal for investigating low-energy nuclear processes and, especially, their spin dependence at low energy. Consider the possible existence of a stable orbit particle pair (necessarily of different particle type) such as deuteron/proton (d, p) or deuteron/helion (d, h), each with laboratory kinetic energy (KE) in the tens of MeV range, and traveling simultaneously with different velocities in the same direction. This periodically enables "rear-end" collision events whose CM KEs can be tuned into the several 100 keV range by changing η_M.

This description is not effective for "same particle" pairs, such as p, p or d, d. Their resultant co-traveling bunch velocities remain identical and no "rear-end" collisions ensue. (Treatment of the fundamentally important case of identical particle scattering has to be deferred for now.)

With careful tuning of E and B, such nucleon bunch pairs will have appropriately different charge, mass, and velocity for their kinematic rigidities to be identical. Both beams can then co-circulate indefinitely, with different velocities.

Depending on the sign of magnetic field B, either the lighter or the heavier particle bunches can be faster, "lapping" the slower bunches periodically, and enabling "rear-end" nuclear collision events. (The only longitudinal complication introduced by dual beam operation is that the "second" beam needs to be injected with accurate velocity, directly into stable RF buckets.)

Only in such a storage ring can "rear-end" collisions occur with heavier particle bunches passing through lighter particle bunches, or vice versa. From a relativistic perspective, treated as point particles, the two configurations just mentioned would be indistinguishable [8]. As observed in the laboratory, to the extent the particles are composite, such collisions would classically be expected to be quite different and easily distinguishable.

Pavsic, in a 1973 paper reproduced in 2001 [9], develops a "mirror matter" Hamiltonian formalism, distinguishing between "external" and "internal" symmetry. He points out, for example, that "the existence of the anomalous proton or neutron magnetic moments indicates the asymmetric internal structure of two particles"; a comment that applies directly to the present paper. Otherwise, Pavsic is agnostic, suggesting that his formalism provides only a parameterization for experiments sensitive to internal structure, with possible implications concerning mirror matter.

4 Proposed E&m ring properties

Specializing the earlier discussion, we limit the electrical and magnetic bending fractions η_E and η_M to satisfy

$$\eta_E + \eta_M = 1, \text{ where } |\eta_M/\eta_E| < 0.1,$$

2024 JINST 19 P11017

where the restriction to predominantly electric bending is arbitrary, not fundamental, and is adopted primarily to simplify discussion in the present paper, especially when bending fraction η_M is small enough to be described as "perturbative". This perturbation "splits" a unique velocity closed circular orbit solution into two slightly separated velocity circular solutions. As a result there are periodic "rear-end" collisions between two particles co-moving with substantially different velocities in the laboratory. Their CM KEs can be in the several 100 KeV range. All incident and scattered particles then have convenient laboratory KEs, two orders of magnitude higher, in the tens of MeV range.

Our proposed "E&m" storage ring is ideal for investigating low energy nuclear processes. With careful tuning of E and B, certain nucleon bunch pairs of different particle type, such as p and d or d and h, can have appropriately different charge, mass, and velocity for their rigidities to be identical. Both beams can then co-circulate indefinitely, with different velocities. For nuclear beams *of different particle type*, depending on the sign of magnetic field B, either lighter or heavier particle bunches will be faster, "lapping" the slower bunches periodically, and enabling "rear-end" nuclear fusion events.

Only in such a storage ring can "rear-end" collisions occur with heavier particle bunches passing through lighter particle bunches, or vice versa. From a relativistic perspective, treated as point particles, the two configurations just described would be indistinguishable. But, as observed in the laboratory, to the extent the particles are composite, such collisions would classically be expected to be quite different or, at least, distinguishable.

Pavsic, in a 1973 paper reproduced in 2001 [9], develops a "mirror matter" Hamiltonian formalism, distinguishing between "external" and "internal" symmetry. He points out, for example, that "the existence of the anomalous proton or neutron magnetic moments indicates the asymmetric internal structure of two particles"; a comment that applies directly to the present paper. Otherwise, Pavsic is agnostic, suggesting that his formalism provides only a parameterization for experiments sensitive to internal structure, with possible implications concerning mirror matter.

5 Storage ring PTR with E&m bending

First suggested by Koop [10], (in the context of counter-rotating proton beams for proton EDM measurement), design of the E&m configuration has been described in a series of papers by or including a present author [2] through [11]. The acronym PTR chosen in ref. [12] to stand for "prototype" has been retained, in spite of the much altered rationale for its existence.

It is possible, with superimposed electric and magnetic bending, for beam pairs of different particle type to co-circulate simultaneously. This opens the possibility of "rear-end" collisions occurring while a fast bunch of one nuclear isotope type passes through a bunch of lighter, yet slower, isotope type (or vice versa). The Pavsic formalism just mentioned seems well suited to the empirical experimental representation of measured differences between these two possibilities.

A schematic diagram of the proposed PTR storage ring is shown in figure 1. PTR lattice description "sxf" files can be obtained at ref. [13]. Though the quadrupole strengths are minimal (as can be seen by the vanishing entrance and exit slopes in figure 2) they have been trimmed for "equal" *fractional* x, y tune values (0.7074, 0.7073).

The optimal thick lens PTR optics (i.e. with quadrupoles essentially turned off, and functioning only for trimming) is uniquely determined, with $m_{\text{nom.}}$ (defined by formulas in figure 5) being curiously close to 1/3, closer to $m = 0$ (cylindrical) than to $m = 1$ (spherical) electrode shape.

2024 JINST 19 P11017

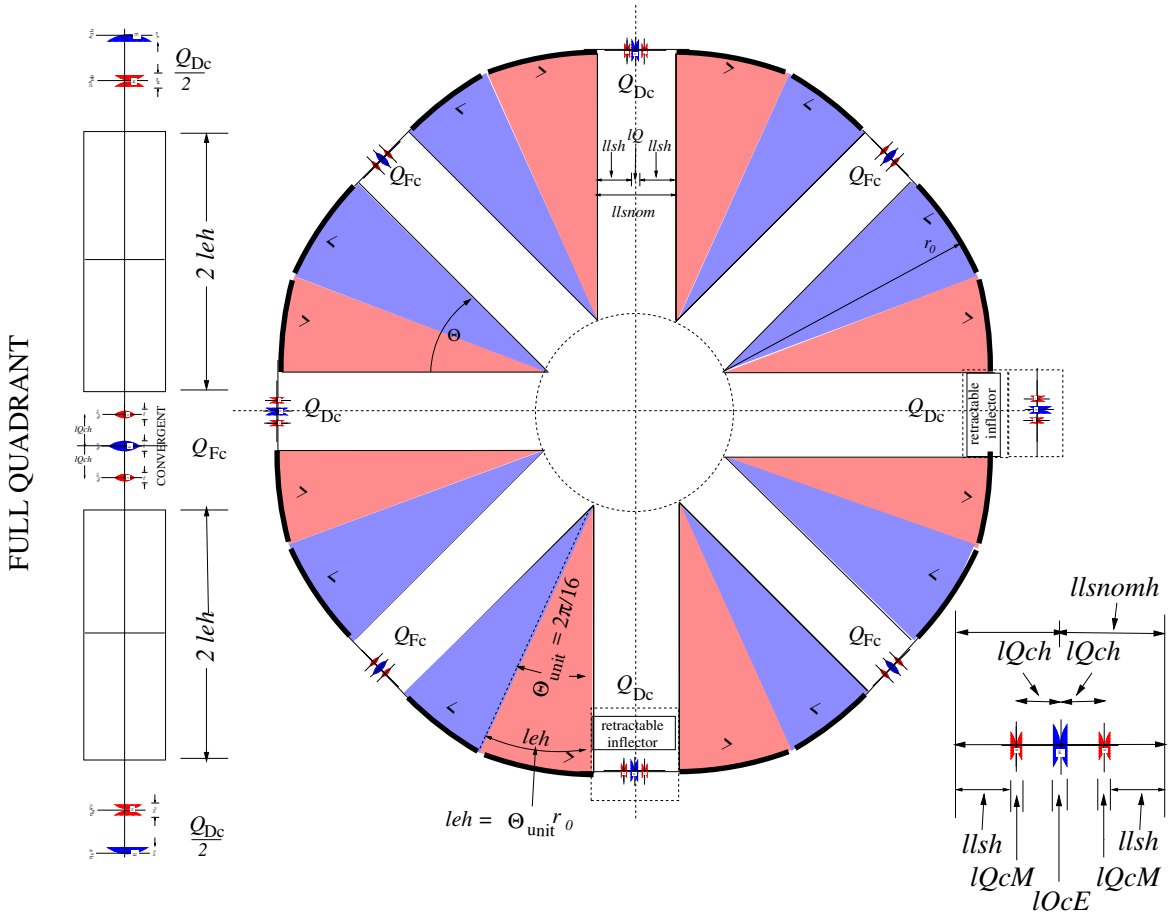

Figure 1. Lattice layouts for PTR, the proposed prototype nuclear transmutation storage ring. "Compromise" quadrupoles [14] are shown lower right. The circumference is 102.2 m. Red/blue alternation indicates individually-powered sectors. (During fabrication, this would permit alternation of the focusing gradients. In situ, it permits the alternation of the sign of E/B. Neither possibility is further discussed in this paper.) The need for a specialized quadrupole "triplet" to implement the E&m superimposed focusing by a "compromise quadrupole" is explained in appendix A of reference [3]. Stated briefly, a "compromise quadrupole" is a split, thick lens, magnetic quadrupole centered on a thin electric quadrupole; both focusing or both defocusing. To linear order this approximates the exact superposition of thin lens electric and magnetic quadrupoles with tunable focusing strengths. To linear order this supports the matching of separated-function quadrupole focusing of forward and backward traveling beams.

With obvious scaling changes, namely electric, E_0/β, and magnetic, cB_0, field strengths varying inversely with the factor qr_0/p, as given in eq. (3.1). *The same focal relationship is valid at all scales, from microscopic to cosmological.* For example, by doubling r_0 to 22 m, the value of E_0 would be reduced from 5.06 MV/m to 2.53 MV/m. See, for example, the central row of table 1.

Bend field stabilization and resettability Electric bend field with superimposed magnetic field is illustrated in figures 3 and 4, the latter of which shows the possible inclusion of soft iron flux return paths. (This would not be acceptable for EDM measurement, because of hysteresis; for low energy nuclear physics this would be much less serious). The designs have been performed by Helmut Söltner, as cited in the figure. Further details are contained in reference [16]

2024 JINST 19 P11017

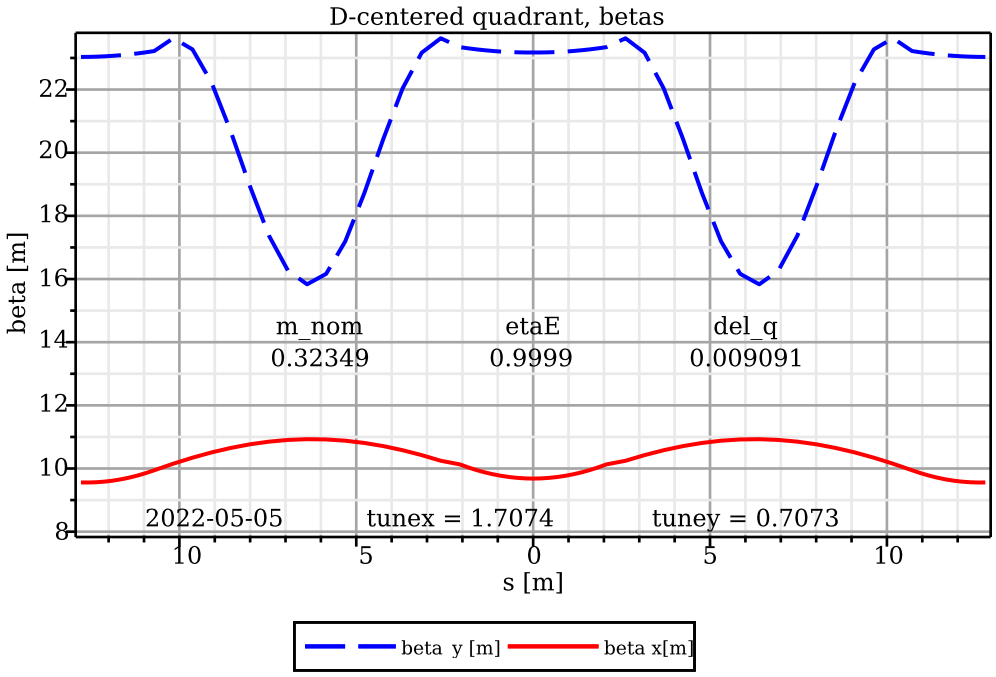

Figure 2. Refined PTR tuning, with quad strengths and $m_{\text{nom.}}$ (adjusted to 0.32349) for (distortion-free) equal-fractional-tune, $Q_x = Q_y + 1$, operation on the difference resonance. Not counting geometric horizontal focusing, thick lens pole shape horizontal and vertical focusing strengths are then identical [15] (mnemonic: $m_{\text{nom.}} = 1/3$). The entire lattice design can be scaled, e.g. to reduce peak field requirements.

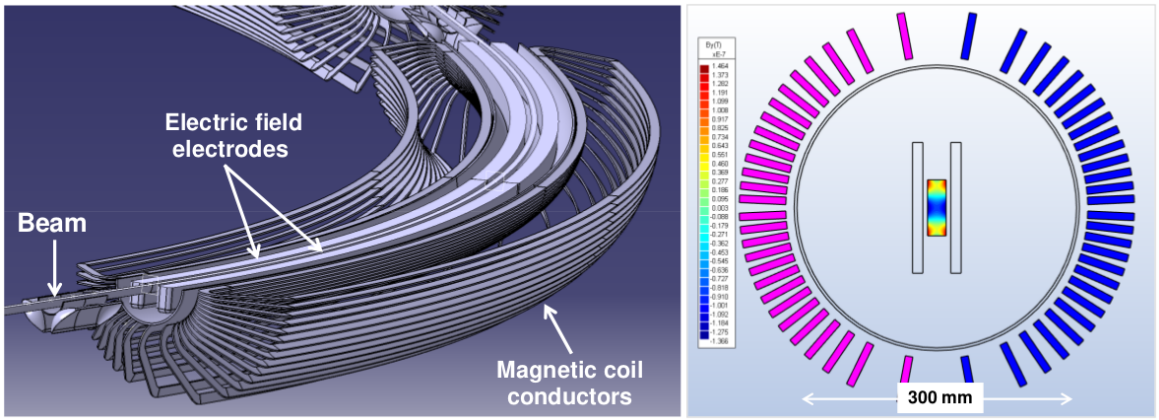

Figure 3. *Left:* cutaway drawing of one sector of the PTR ring bending element. *Right:* a transverse section showing an end view of the (inner legs of the) magnet coil, as well as a field map of the good field region. The (brilliant) design is due to Helmut Söltner [12]. The magnet is "air core", limited to quite weak magnetic field, but sufficient for most applications. Current design maximum values for electric and magnetic fields are 10 MV/m and 30 mT.

2024 JINST 19 P11017

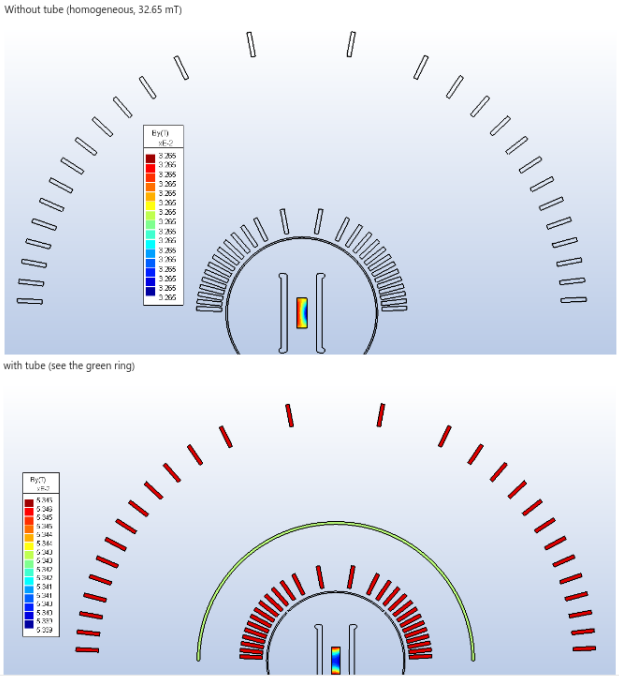

Figure 4. *Top* full transverse section of top half of the air core bending element shown on the right in figure 3. *Bottom:* full transverse section of top half of an iron-enhanced version of the bending element shown on the right in figure 3. For predominant magnetic, e&M, bending, the lower design would be required. This design has been graciously provided by Helmut Söltner.

When contemplating the high precision measurement of nuclear parameters, especially their anomalous magnetic moments G, one assumes that all intentional electric and magnetic field components are known with high precision and all unintentional field components are known to vanish with high accuracy. The degree to which this can be achieved in a "small" accelerator, say of 100 m circumference, needs to be established.

Though it is possible to measure both magnetic and electric field components to high accuracy in many locations, it is not possible to make such measurements exactly along the storage ring design central orbit. In this respect, polarized beams can come to the rescue.

As regards the orientation of the beam polarization, it is essential to distinguish between "in-plane" and "out-of-plane" orientations, where "the plane" refers to the ring beam plane, which is presumed to be horizontal. *In-plane precession*, induced by ideal magnetic fields acting on beam particle magnetic dipole moments (MDMs) is routinely the dominant spin precession.

Assuming the absence of non-zero electric dipole moments (EDMs) as is required by time reversal invariance, *out-of-plane precession* can be induced only by electric or magnet field imperfection — radial, in-plane magnetic field components or vertical out-of-plane electric field components. In practice, the inevitable existence of unintentional fields acting on particle MDMs will induce out-of-plane precession. The radial magnetic field average or the $\langle B_r \rangle$ and the vertical electric field $\langle E_y \rangle$ average are expected to be the dominant source of spurious MDM-induced precession.

The leading strategy for setting and resetting conditions will be to monitor the beam polarizations to feedback-stabilize the beam polarizations. Before this, however, this condition can be achieved by adjusting local beam deflection components; $\langle B_r \rangle$ can be canceled by canceling the out-of-plane

2024 JINST 19 P11017

(vertical) orbit separation of (sequential) counter-circulating beams. (Hysteresis in the possible soft iron cylinder mentioned previously would impair this compensation significantly.) We refer to this capability as "self-magnetometry". The precision with which the orbits can be matched vertically depends on the precisions of the beam position monitors (BPMs) that measure the vertical beam positions, and on the ring lattice sensitivity to the magnetic field errors causing the orbits to be vertically imperfect. Because of the weak vertical focusing this sensitivity is excellent.

Assuming both beam spins are frozen, at least the "primary" beam-1 will, by convention, be globally frozen, with spin tune $Q_{s1} = 0$. The presence of magnetic bending guarantees that this condition can be satisfied. Ideally both beams would have $Q_s = 0$ but, with only a few exceptions, the "secondary" beam-2 can only be locally frozen; Q_{s2} exactly equal to a rational fraction other than $0/1$.

In this condition both beam polarizations can be phase-locked, allowing both beam spin tunes to be set and re-set with frequency domain precision. This means that synchronism can be maintained for runs of arbitrary duration. Since the RF frequency can also be restored to arbitrarily high precision, conditions can be set and re-set repeatedly, without depending upon high precision measurement of the electric and magnetic bend fields.

This also allows, for example, the magnetic bending field to be reversed with high precision, as would be required to interchange CW and CCW beams. This capability can be referred to as *stabilizing all fields by phase locking both revolution frequencies and both beam polarizations, using their own MDMs as "magnetometric gyroscopes"*.

5.1 Tentative BNL site

To indicate the size scale of the proposed PTR ring a tentative site location at Brookhaven National Laboratory (BNL) is shown in figure 6. Most of the nuclear isotope beams mentioned in this paper can be made available at suitable power levels in that vicinity [17]. What makes this important is that the cost of producing these isotope beam sources from the ground up would greatly exceed the PTR implementation cost (except at BNL or any other lab with suitable isotope beams).

6 Longitudinal beam dynamics

PTR longitudinal beam dynamics is discussed in detail in reference [3]. The following synchrotron oscillation figures are copied from that source.

Figure 7 shows the dependence of synchrotron tune Q_s upon RF voltage V_{RF}.

Figure 8 shows the dependence of bunch length upon RF voltage V_{RF}.

Figure 9 plots the fractional momentum offset δ against turn number for a sequence of RF voltages.

Figure 10 displays longitudinal phase space plots for the same series of RF voltages.

The condition for bunch collision points to occur at fixed ring locations is met by the beam velocities being in the ratio of integers; e.g. $\beta_1/\beta_2 = 8/7$ in table 1. *Both circulating beams can be bunched by a single RF cavity in spite of their different velocities.*

With 8/7 velocity ratio and $7 \times 8 = 56$, the RF frequency can be the 56th harmonic of a standard base frequency, f_{base}, itself a harmonic number h_n multiple $f_{\mathrm{base}} = h_n f_{\mathrm{rev.}}$ of the revolution frequency. Stable buckets are labeled for simple cases in figure 11. (Hint: when the second indices are both zero, the populated bunches superimpose.) A "remote" bunch collision point appears on the left, but not on the right.

2024 JINST 19 P11017

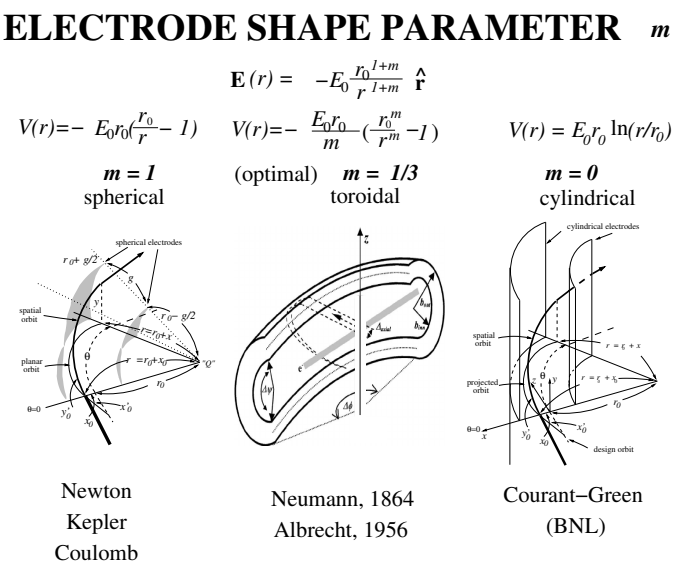

Component	Cost (k€)
Bends	9200
Electric quads	1700
Vacuum	1800
Pick-ups	900
Control	1500
Polarimeter	1200
RF equipment	300
Total	16600

Figure 5. *Left:* Electrode shapes are shown with their focusing strength parameters m, for spherical, (optimized) toroidal, and cylindrical bending fields. [11, 18–20] *Right* 2021 CERN Yellow report cost estimate [12] for the apparatus shown in figure 3.

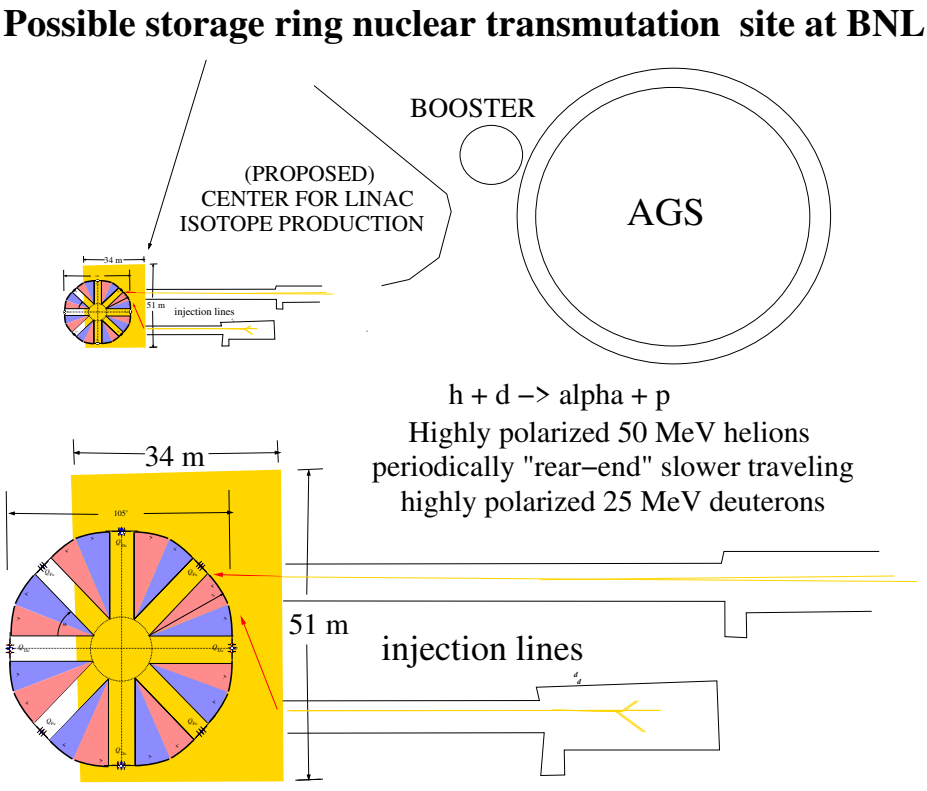

Figure 6. *Above* Tentative PTR location near the AGS at BNL, using existing, high current isotope sources. *Below:* Magnified image insert of PTR complex.

2024 JINST 19 P11017

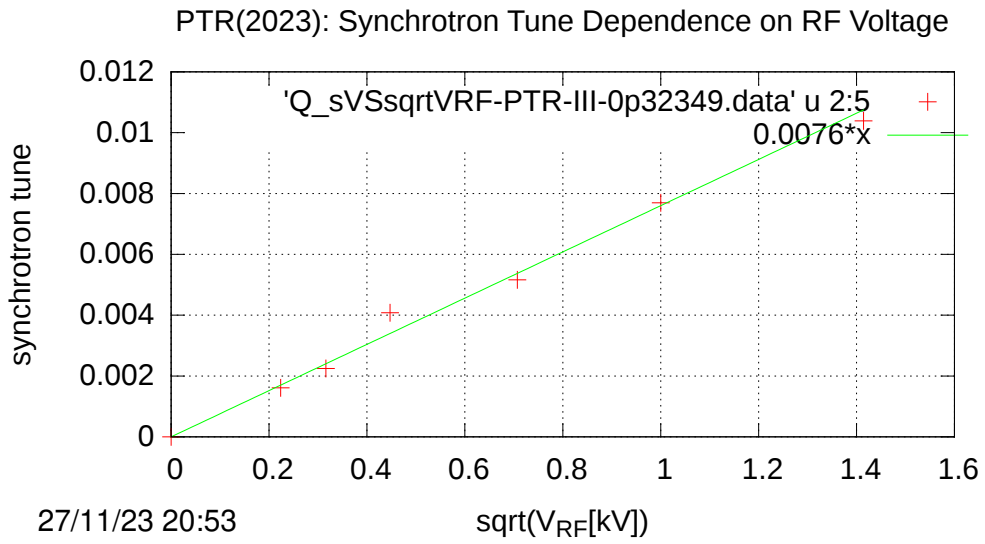

Figure 7. Plot of synchrotron tune Q_s (obtained by counting periods in plots like those in figure 9) versus $\sqrt{V_{\rm RF}[\rm kV]}$. The fit yields $Q_s = 0.0076\sqrt{V_{\rm RF}[\rm kV]}$.

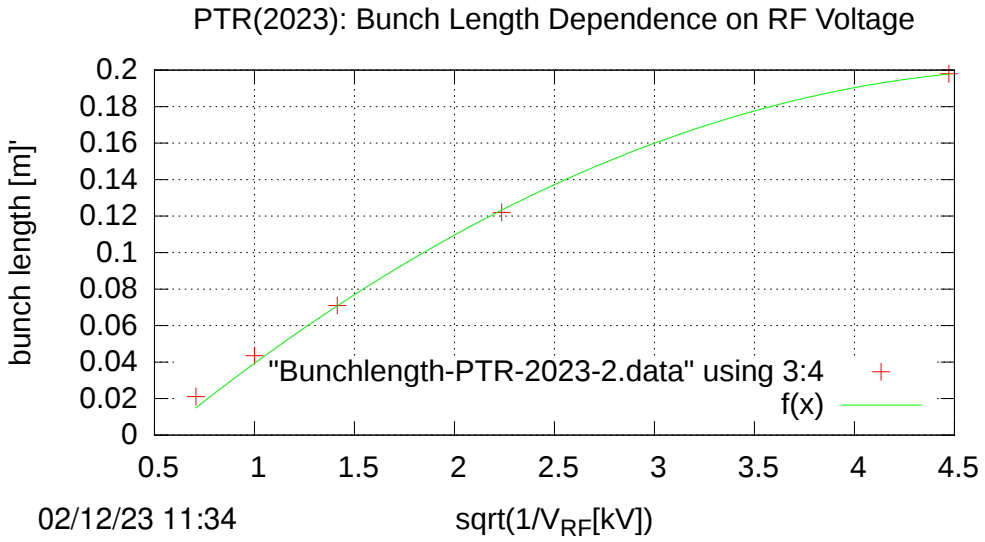

Figure 8. Plot of bunch length (extremes in plots like those in figure 10 for $\delta_{\rm UAL}$=0.000003) versus $\sqrt{1/V_{\rm RF}[\rm kV]}$. The best fit in the form b.l. $= f(x) = a + b * (x - 0.7071) + c * (x - 0.7071) * *2$, has $b = 0.086 + /-0.0039$, $c = -0.00996 + /-0.0011$. For example, the bunch length for 1 KV RF voltage is 4 cm.

7 Nuclear physics investigation with E&m storage ring

7.1 "Rear end" collisions: $h + d \rightarrow \alpha + p$

"Rear-end" collisions occurring during the passage of faster bunches through slower bunches can be used to study spin dependence of nucleon, nucleon collisions in a semi-relativistic moving coordinate

2024 JINST 19 P11017

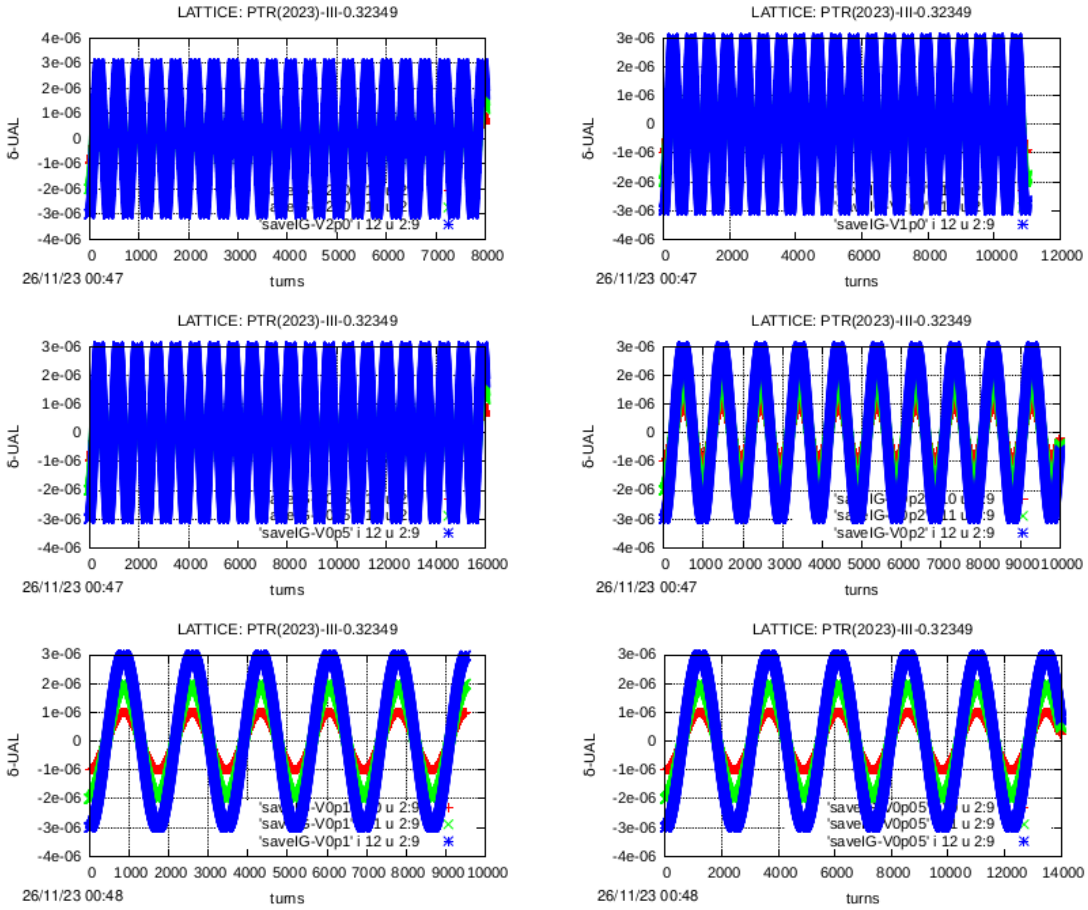

Figure 9. Fractional offset $\delta_{\mathrm{UAL}} \equiv \delta\mathcal{E}/(p_0 c)$ plotted against turn number for values of RF amplitude $\hat{V}_{\mathrm{RF}}$: 2.0, 1.0, 0.5, 0.2, 0.1, 0.05 [kV]—reading from left to right then top to bottom; lattice `PTR(2023)-III-0.32349`. Each of the plots shows three synchrotron oscillation amplitudes (with the lower amplitude data largely obscured by the (blue) large amplitude data). Starting from the origin with vanishing slopes, the initial "momentum offsets" are $\delta_{\mathrm{UAL}} = -0.000001, -0.000002$, and -0.000003. The number of turns tracked in each case is a (large) multiple of 100, which is also close to a quarter-integer synchrotron tune advance, aliasing ambiguities are avoided. These plots provide the synchrotron tune values plotted in figure 7.

frame. Such rear-end collisions allow the CM KEs to be in the several 100 KeV range, while all incident and scattered particles have convenient laboratory KEs, two orders of magnitude higher, in the tens of MeV range.

This permits incident beams to be established in pure spin states and the polarizations of scattered particles to be measured with high analyzing power and high efficiency; Wilkin [21], Lenisa, et al. [22]. In this way the E&m ring satisfies the condition that all nuclear collisions take place in a coordinate frame moving at convenient semi-relativistic speed in the laboratory, with CM KEs comparable with Coulomb barrier heights.

As a first nuclear physics example, this paper concentrates on d and h beams co-circulating concurrently in the same storage ring, with parameters arranged such that, in the process $d + h \rightarrow p + \alpha$, rear-end collisions always occur in a detector at the intersection point (IP). Detector details are presented in appendix B of reference [3].

2024 JINST 19 P11017

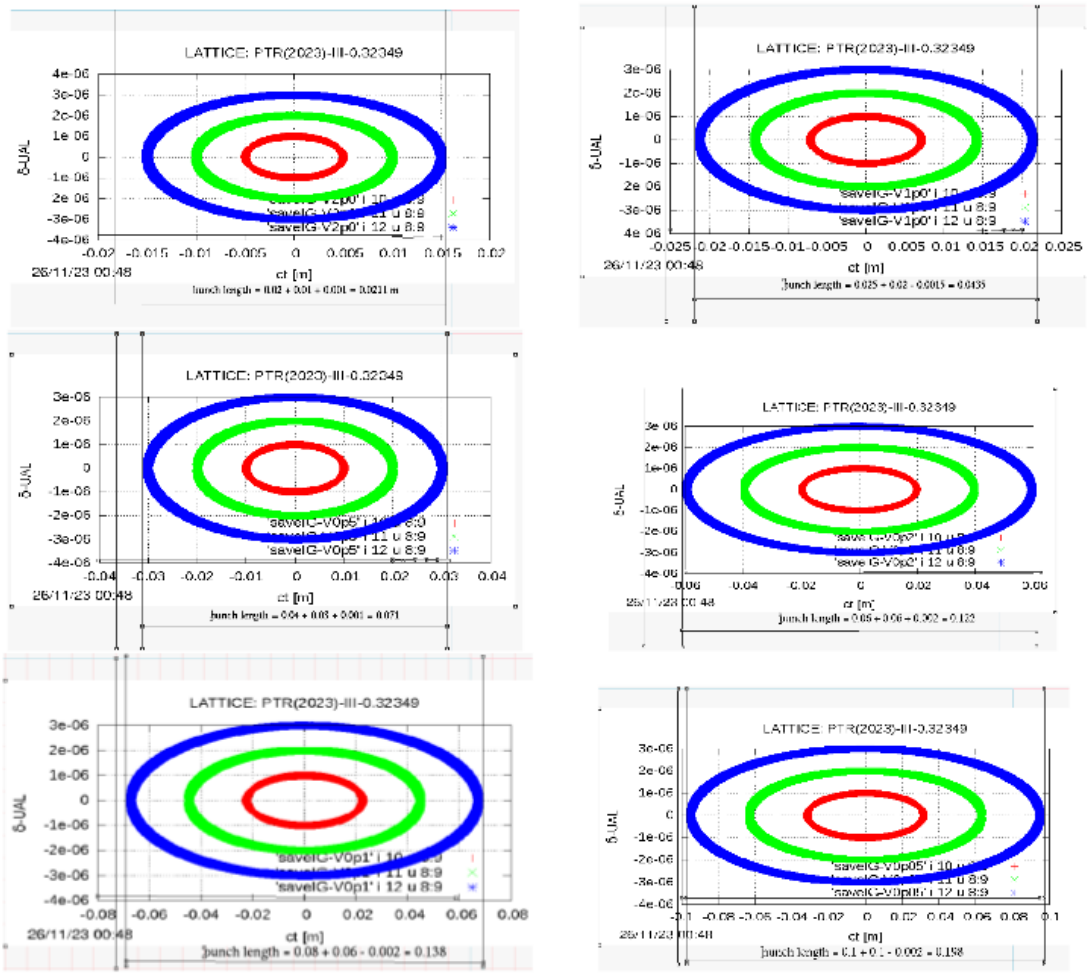

Figure 10. Longitudinal phase space plots for the same series of RF voltages, 5.0, 2.0, 1.0, 0.5, 0.2, 0.1, 0.05 [kV] as in figure 9. The horizontal axis is z in meters. The vertical axis is the fractional offset $\delta\mathcal{E}/(p_0c)$ These plots provide the bunch length values plotted in figure 8.

(In a conventional (magnetic) contra-circulating colliding beam storage ring the energy would be above the pion production threshold, with production into this transmutation channel negligibly small.)

Consider d and h beams co-circulating concurrently in the same storage ring, with parameters arranged such that, in the process $d + h \rightarrow p + \alpha$, rear-end collisions always occur in the detector at an intersection point (IP). The center of mass kinetic energies (where their momenta are equal and opposite) have been adjusted to be close to the Coulomb barrier height for this nuclear scattering channel. With judicious adjustment, all nuclear events will occur at the ring intersection point (IP) of a full acceptance interaction detector/polarimeter. Such a device is illustrated schematically in figure 25 of reference [3].

In this configuration the rest mass of the h, d system will be fine-tunable on a KeV scale, for example barely exceeding the threshold of the $h + d \rightarrow \alpha + p$ channel, but below pion production and other inelastic thresholds. Tentatively neglecting spin dependence, the expected radiation pattern can be described as a "rainbow" circular ring (or rather cone) formed by the more massive (α-particles) emerging from, and centered on, the common beam axis. This "view" has not been observed previously in nuclear measurements since it requires a "rear end" collision.

2024 JINST 19 P11017

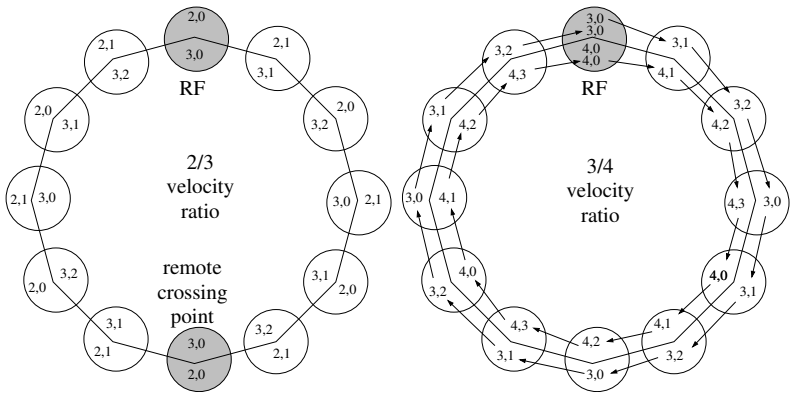

Figure 11. Stable RF buckets for beam velocity ratios of 2/3 or 3/4. Shaded circles indicate locations at which bunch positions coincide. The undesirable collisions at the RF location should be removable with symmetrically split RF locations; i.e. with no RF cavity at the "effective cavity location" labelled "RF" in the figure.

Consider d and h beams co-circulating concurrently in the same storage ring, with parameters arranged such that, in the process $d + h \rightarrow p + \alpha$, rear-end collisions always occur in the detector at an intersection point (IP). The center of mass kinetic energies (where their momenta are equal and opposite) are close to the Coulomb barrier height for this nuclear scattering channel. With judicious adjustment, all nuclear events will occur at the ring intersection point (IP) of a full acceptance interaction detector/polarimeter.

Table-1 provides kinematic parameters for the $h + d \rightarrow \alpha + p$ channel. The first and last columns identify incident beams h and d as beams 1 and 2. Columns 2, 3, 4 contaim beam 1 parameters; column 5 gives the electric field, and column 6 gives the magnetic bending fraction $\eta_M 1$ (not the same as for particle 2); columns 7,8,9 contain beam 2 parameters; the remaining columns give CM quantities, which are identified by asterisks "*". The point of this table is that the number 8.00015, the final entry in the middle row, is close enough to the integer 8 to permit phase-locking to exactly 8; this locks the bunch collisions occurring every 8th turn of the faster particle to a fixed (but adjustable) ring location.

The columns labeled Q_s are spin tunes. In this paper nothing, beyond spin tune entries Q_s in various tables, is said about polarization; but *support for scattering highly polarized beam particles with high quality final state polarimetry capability provides the main motivation for the proposed E&m project.*

The electric/magnetic field ratio produces perfect $\beta_h/\beta_d = 8/7$ velocity ratio so that, for every 7 deuteron turns, the helion makes 8 turns. Notice, also, the approximate match of Q12=317 KeV in this table, with Coulomb barrier energy, $V_{d,He3} = 313.1$ KeV. This matches the incident kinetic energy to the value required to surmount the repulsive Coulomb barrier.

Temporarily neglecting spin dependence, the expected radiation pattern can be described as a "rainbow" circular ring (or rather cone) formed by the more massive (α-particles) emerging from, and centered on, the common beam axis. This "view" has not been observed previously in nuclear measurements since it requires a "rear end" collision. The $h + d \rightarrow \alpha + p$ nuclear transmutation channel, are illustrated as "rainbows" in figure 12.

As already stated, in this paper little more is said about polarization, but support for scattering highly polarized beam particles with high quality final state polarimetry capability provides a major motivation for the proposed E&m project, and Q_s continues to be exhibited in tables.

2024 JINST 19 P11017

Table 1. Fine-grain scan to center the collision point for co-traveling KE1=49 MeV helion energy and 24.9 MeV deuteron energy. With velocity ratio 8/7, multiplying by 7 produces the central entry in second last column. The bend radius is $r_0 = 11$ m.

bm 1	β_1	Qs1	KE1 MeV	E0 MV/m	η_{M1}	β_2	Qs2	KE2 MeV	$\beta*$	$\gamma*$	$M*$ GeV	Q12 KeV	$7\beta_1/\beta_2$	bm 2
h	0.1826	−0.666	48.000	4.961 39	−0.146 62	0.1597	−1.097	24.391	0.173 43	1.015 39	4.684 32	311.214 68	8.000 83	d
h	0.1844	−0.666	49.000	5.067 42	−0.147 42	0.1613	−1.098	24.901	0.175 19	1.015 71	4.684 32	317.546 05	8.000 15	d
h	0.1862	−0.666	50.000	5.173 55	−0.148 22	0.1630	−1.098	25.410	0.176 93	1.016 03	4.684 33	323.871 33	7.999 47	d

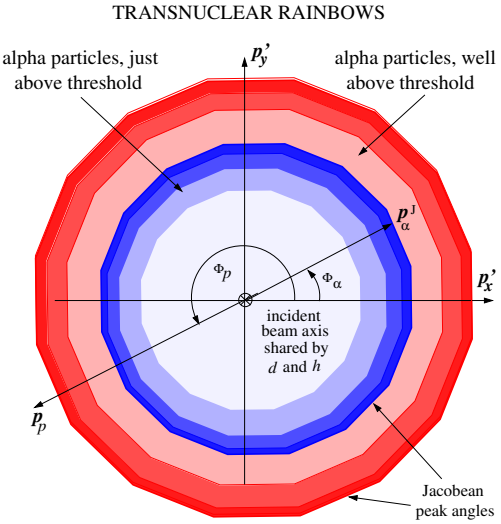

Figure 12. Transnuclear "rainbows" produced in the reaction $h + d \rightarrow \alpha + p$. Shading represents scattered differential cross section. Rainbow radii increase proportional to incident energy excess above threshold. Superscript "J" labels the rainbow divergence edge caused by the vanishing Jacobean at the laboratory scattering angle maximum. Jacobean peak "rainbow" production patterns for the nuclear transmutation process $h + d \rightarrow \alpha + p$. The $p + d \rightarrow h + \gamma$ channel would exhibit only a single, more acute angle h rainbow. For correlation with, say, terrestrial rainbows, refer to Van-de-Hulst [23]. For actual rainbows a further empirical numerical factor, $\pi(m - 1)$ of order 1, multiplying the diameter, is required, where m is "index of refraction".

The electric/magnetic field ratio produces perfect $\beta_h/\beta_d = 8/7$ velocity ratio so that, for every 7 deuteron turns, the helion makes 8 turns. Notice, also, the approximate match of Q12 = 317 KeV in this table, with Coulomb barrier energy, $V_{d,\mathrm{He3}}$=313.1 KeV. This matches the incident kinetic energy to the value required to surmount the repulsive Coulomb barrier.

7.2 Rate calculation: $h + d \rightarrow \alpha + p$

In this case the β-ratio is 7/8. Typical parameters include

$$
\begin{aligned}
f_{\mathrm{sr}} &= \text{ring proton revolution frequency} = 1 \times 10^6\ \mathrm{Hz},\\
N_d, N_h &= \text{numbers of stored particles} = 10^{11},\\
A_b &= \text{beam area} = 0.1\ \mathrm{cm} \times 0.1\ \mathrm{cm} = 1 \times 10^{-2}\ \mathrm{cm}^2,\\
\sigma &= \text{nuclear cross section} = 1 \times 10^{-24}\ \mathrm{cm}^2\,.
\end{aligned}
$$

The (deuterium) "target bunch nuclear opacity" is

$$O_{\rm N} = N_d \sigma / A_b = 10^{11} \times 10^{-24} / 10^{-2} = 10^{-11} \,,$$

which gives the fraction of particle passages that results in a nuclear event. The rate of particle passages is

$$r_{\rm pass} = \frac{f_{\rm sr}}{7} N_h = \frac{10^6}{7} \times 10^{11} = 0.142 \times 1 \times 10^{17}\ {\rm s}^{-1}.$$

The resulting nuclear event rate is

$$r_{\rm event} = O_{\rm N} \times r_{\rm pass} = 10^{-11} \times 0.142 \times 10^{17} = 1.42 \times 10^5\ s^{-1}\,.$$

Figure 13 contains a laboratory frame momentum diagram for the process. Rolled around the longitudinal axis, the figure is intended to show how azimuthal symmetry imposes the rainbow scattering pattern shown in figure 12, with cone angle increasing proportional to the incident energy excess over threshold energy.

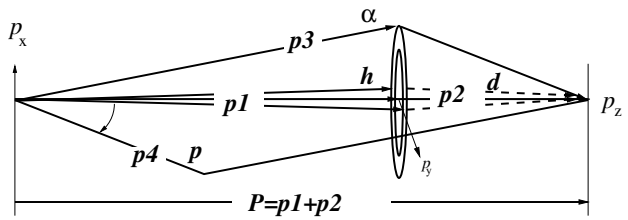

Figure 13. Laboratory frame momentum vector diagram. The vector $\mathbf{P} = \mathbf{p_1} + \mathbf{p_2}$ is the sum of the lab momenta of one particle from beam 1 (h) and one from beam 2 (d). Scattered alpha particle direction (3) is shown above the beam axis; the scattered proton direction (4) would then be below, as displayed by parallelogram construction.

7.3 "Rainbow", "rear-end" $d + h \rightarrow p + \alpha$ collisions

Here we consider $d + h \rightarrow p + \alpha$ "elastic" (including weakly inelastic) scattering in the E&m storage ring. d and h beams co-circulate concurrently with different velocities in the same ring, such that "rear-end" collisions always occur at the same intersection point (IP). The CM kinetic energies are to be varied continuously, keV by keV, from below the several hundred keV Coulomb barrier height, through the (previously inaccessible for spin control) range up to tens of MeV and beyond. With the scattering occurring in a moving frame, initial and final state laboratory momenta are in the convenient tens of MeV range.

All nuclear events occur within a full acceptance interaction detector/polarimeter discussed in appendix B of reference [3]. Temporarily neglecting spin dependence, the CM angular distributions will be approximately isotropic [24, 25]. (Especially with heavier particles being faster) most final state particles end up traveling "forward" to produce "rainbow" circular rings (or rather cones) formed by the final state particles. (In the absence of "rear-end" collisions) this "view" has yet to be self evident in nuclear scattering experiments.

Figure 14 shows the dependence of final state laboratory proton and alpha particles KEs upon CM angle.

In recent years there have been many developments in beam polarization control and in polarimetric spin orientation detection, many of which have been produced at the COSY storage ring in Jülich, Germany, including Wilkin [21], Eversman [26], Hempelmann [27], Rathmann, [28], Slim, [29], and Rathmann [30].

2024 JINST 19 P11017

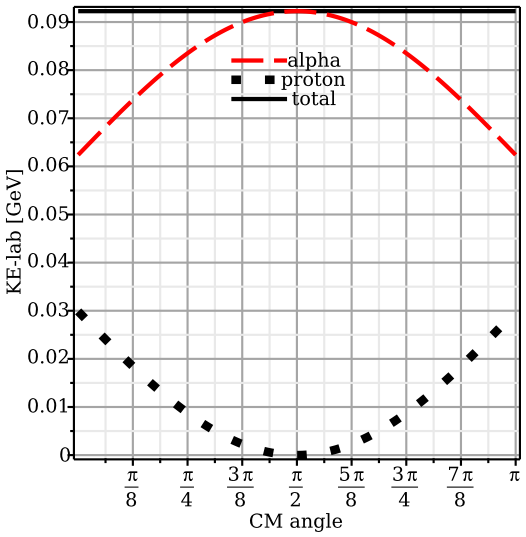

Figure 14. Plot of lab KEs vs c.m. angle for the $h + d \rightarrow \alpha + p$ process.

8 Positron induced triton two-body β-decay

There is much more to be said concerning conventional low energy nuclear physics, especially concerning the exploitation of spin control and polarization measurement. We turn, however, to the less well understood weak nuclear interaction area. This does not imply that the experimental methods already explained will need to be greatly altered, though with significantly different particle detection and polarimetry.

Figure 15 illustrates the kinematics of the $t + e^+ \rightarrow h + \nu$ channel in the form of a graph relating initial state CM polar angles final state lab polar angles. Figure 16 plots final state kinetic energies vs CM polar angles.

Table 2 shows lab parameters for helions and tritons following identical orbits, with h as master (beam 1) on the left and t as beam 2 on the right, and shared field values in the middle. Note, in this case, because of almost identical masses, but charges differing by a factor of two, that the magnetic bending is strong and destructive in both cases.

Table 2. Co- and contra-rotating closed orbit solutions, distinguished respectfully by the sign of beta2 in the two rows, with matching h and t beam parameters. Notice, unusually in this table, that the sign of β_2 is opposite in the two rows.

bm 1	m1 GeV	G1	q1	β_1	Qs1	KE1 MeV	E0 MV/m	etaM1	m2 GeV	G2	q2	β_2	KE2 MeV	bratio	Qs2	bm 2
h	2.8084	−4.1842	2	0.1519	4.233×10^{-1}	33.0	4.4131	−0.4796	2.8089	7.915	1	−0.150 20	32.2316	−0.9884	1.331	t
h	2.8084	−4.1842	2	0.1516	4.233×10^{-1}	33.0	4.4131	−0.4796	2.8089	7.915	1	0.113 99	18.4302	0.750 13	−3.736	t

Because the process is exothermic, the sum of scattered kinetic energies, as well as being independent of scattering angle, exceeds the sum of initial state laboratory kinetic energies. However, the helion and neutrino shares of lab kinetic energy are comparable, within a factor of two, as figure 16 shows.

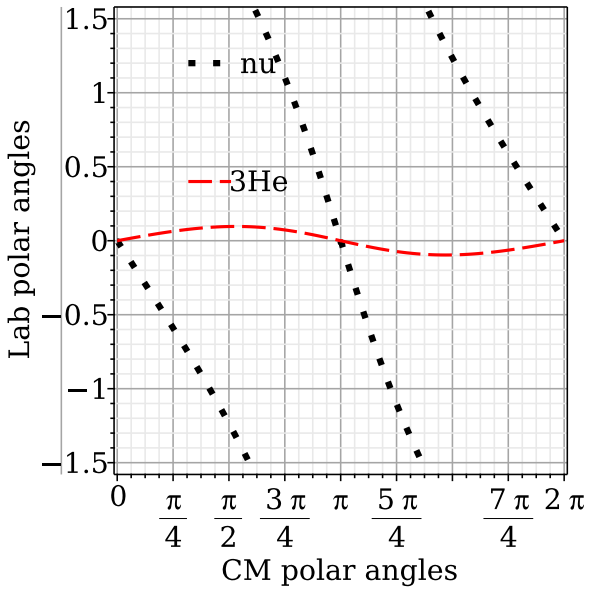

Figure 15. Plot of lab polar angles vs CM polar angles for the e^+ + triton final state 3He + ν channel. Notice that, viewed in the laboratory, the produced helions are reasonably well collimated, while the (invisible) scattered neutrinos are more or less isotropic.

In reconstructing the two-body kinematics, the only significant theoretical unknown is the neutrino rest mass. Both incident beam energies can be measured and controlled with 9 (and probably more) decimal point accuracy, as demonstrated at COSY in reference [27], along with exactly forward momentum. To the extent that final state helion direction and momentum can be perfectly measured, the neutrino rest mass can be inferred. The kinematic constraints and correlations make this issue too complicated for significant assessment in the present paper.

Unlike existing neutrino mass determinations, this neutrino mass measurement is sensitive to the neutino mass itself (which could, in principle, be imaginary), rather than to its square (which could, in principle, be negative). Clearly no single event can be measured with accuracy competitive with currently known neutrino mass upper limits [36]. But a significantly large fraction of the scattered helions populate the "limb of the rainbow", barely inside the Jacobean peak of the rainbow cone. Statistically, this can reduce the neutrino mass error limits.

An alternative way of assessing the impact of this statement, based on the already experimentally established upper limit of order 1 eV^2 for the neutrino mass-squared, is that, to all intents and purposes, other than for measuring the neutrino mass, the kinematics satisfies, exactly, two-body kinematics with one of the final state particles essentially massless. All these comments apply equally to the inverse process, $h + e^- \rightarrow t + \nu$, discussed in the next section.

For visualizing the angular distribution of scattered particles, one should roll both curves in figure 15 around the longitudinal axis, anticipating cylindrical symmetry, at least to the extent that spin dependence can be neglected.

Unlike p, p scattering, because the positron mass is so small, the Rutherford scattering should not be important, even in near-forward directions. As a consequence most of the scattered helion foreground will be essentially free of background radiation. On the other hand, in spite of the quite low positron kinetic energy, the determination of neutrino rest mass may require radiative correction.

2024 JINST 19 P11017

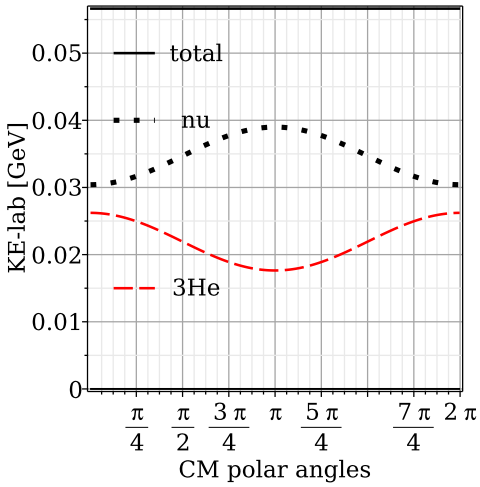

Figure 16. Plot of final state kinetic energies vs CM polar angles for the e^+ + triton final state 3He + ν channel.

Except at very small angles the signature of scattered helions should permit the foreground to be easily distinguishable from the background. Note though, that the largest helion laboratory angle will never exceed a small angle less than 15 degrees.

8.1 Polarimetry of "β-decay process" helions

During initial investigation of induced tritium β-decay it will not be possible to measure the energy of the produced helions with the precision necessary for the precise determination of the neutrino mass. It will, however, be possible to measure the spin dependence of this weak interaction channel. As explained previously, the initial spin states can be pure and the final spin polarizations measured with high efficiency and high analyzing power.

Table 3 provides initial state and center of mass kinetic parameters for "positron induced triton two-body β-decay".

Table 4 shows, line-by-line, the fine tuning required to cause rear-end collisions to occur at the IP for "positron induced triton two-body β-decay".

Table 5 shows final state kinematic parameters for "positron induced triton two-body β-decay".

Table 3. Field strengths, kinematic data, and spin tunes for the initial state of the reaction $e^+ + t \rightarrow h + \nu$.

bm	m1	G1	q1	beta1	Qs1	KE1	E0	etaM	m2	G2	q2	beta2	KE2	bratio	Qs2	bm
1	GeV					MeV	MV/m		GeV				MeV			
t	2.8089	7.9150	1	0.111 74	-7.965×10^{-1}	17.7020	3.1730	0.3170	0.0005	0.0012	1	0.999 91	37.8856	8.9485	7.502×10^{-2}	pos

Table 4. Finely-tuned field strengths, kinematic data, and spin tunes for the reaction $e^+ + i \rightarrow h + \nu$.

bm	beta1	Qs1	KE1	E0	etaM	beta2	Qs2	KE2	beta*	gamma*	M*	Q12*	9*bratio	bm
1			MeV	MV/m				MeV			MeV	KeV		2
t	0.1108	−0.796	17.400	3.118 42	0.011 25	0.9999	0.074	37.321	0.122 54	1.007 59	2.842 57	33 136.769 39	0.997 22	pos
t	0.1111	−0.796	17.500	3.136 50	0.011 18	0.9999	0.074	37.508	0.122 90	1.007 64	2.842 72	33 291.477 09	1.000 06	pos
t	0.1114	−0.796	17.600	3.154 60	0.011 11	0.9999	0.075	37.695	0.123 27	1.007 69	2.842 88	33 445.986 81	1.002 88	pos

2024 JINST 19 P11017

Table 5. Final state kinematics of the reaction $e^+ + t \rightarrow h + \nu$.

bm 3	m3 GeV	G3	q3	th3-90	th4-90	KE3 MeV	E0 MV/m	etaM	KE4 GeV	m4	G4	q4	bm 4
h	2.8084	−4.1834	2	8.64	−111.14	21.93	3.1730	0.0110	34.6981	0.0000	0.0000	0	ν

9 Electron induced triton β-reincarnation

For various reasons, there is another permutation of the input and output weakly interacting particles that seems more favorable experimentally; namely $e^- + h \rightarrow t + \nu$. This channel could be referred to as *electron induced triton two-body β-reincarnation*. In traditional nuclear physics terminology the process would be referred to as *electron capture* (EC) or *internal conversion*.

As explained in appendix F of reference [3], the quartic orbit equation is satisfied by the design orbit of every circular storage ring with arbitrarily superimposed E&M bending.

One might suppose that a predominantly magnetic ring, like an e^+/e^- collider, would be needed to store positive and negative beams at the same time. This is not correct in our case, however. For one thing, to obtain rear-end collisions both beams must travel in the same direction. Also, though inconvenient, what makes it possible with predominantly electric bending, in our case, is that electrons are three orders of magnitude lighter than helions.

For the experiment to work, a negative (electron) beam and a positive (He3) beam have to circulate in the same direction. This means the magnetic field bending has to be destructive in its effect on the He3 beam. So, the electric field has to be stronger than it would be with no magnetic field. Because of its charge being +2, the He3 has a two-fold advantage as regards the electric bending force, and it is also slow, not very responsive to the wrong sign magnetic field.

The magnetic field is constructive in its effect on the electron beam. Fortunately, the electron velocities are four times greater than the helion velocities. As a result, the (constructive) magnetic force on the electrons is two times greater than is the (destructive) magnetic force on the helions.

The net effect is that the bending is centripetal in both cases, even though it is destructive in both cases as regards the coherency of electric and magnetic contributions.

The He3 bending remains, therefore, predominantly electric, but stronger than would be needed to store just the helions. It may be, therefore, that the ring circumference needs to be increased from its 102.5 m current value, but that the current superposition design of figure 3 may remain unchanged.

In the context of the present paper, in contrast with the *status quo,* the primary distinction is that the initial electron would be under direct experimental control, both in kinetic energy and spin orientation. This causes initial state visualization to be more particle-like than wave-like.

There are other considerations, mainly concerning event rate, that makes the $e^- + h \rightarrow t + \nu$ channel more attractive than the $e^+ + t \rightarrow h + \nu$ channel. One is that intense polarized helion beams are already available — for example at BNL [31]. Another is that electron beams are easy, positron beams are difficult.

Figures 17 and 18 demonstrate kinematic dependencies for "electron-induced triton beta reincarnation" and can be compared to figures 15 and 16, which show correspoding kinematic dependencies for "positron induced triton two-body β-decay".

Table 6 provides initial state kinetic parameters for "electron induced triton β-reincarnation".

Table 7 shows, line-by-line, the fine tuning required to cause rear-end collisions to occur at the IP for "electron induced triton β-reincarnation".

2024 JINST 19 P11017

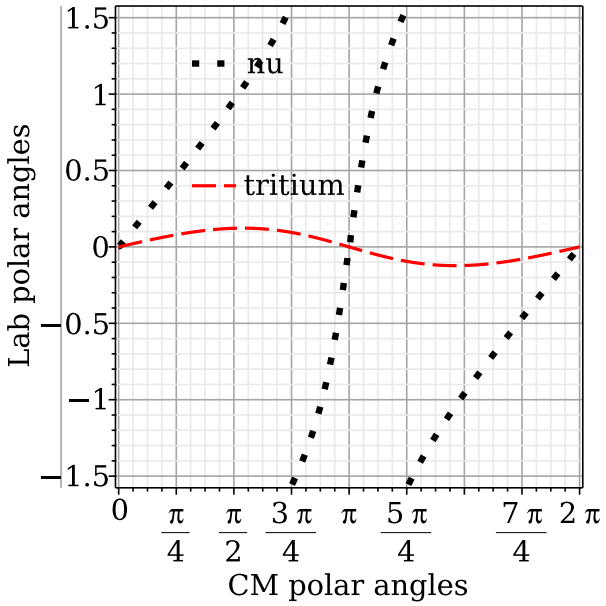

Figure 17. Plot of lab polar angles vs CM polar angles, for the final state of the reaction $e^- + 3\text{He} \rightarrow \text{triton} + \nu$. Both incident beams are at (0,0) in this plot. Notice that, viewed in the laboratory, the produced helions are reasonably well collimated, while the (invisible) scattered neutrinos are more or less isotropic.

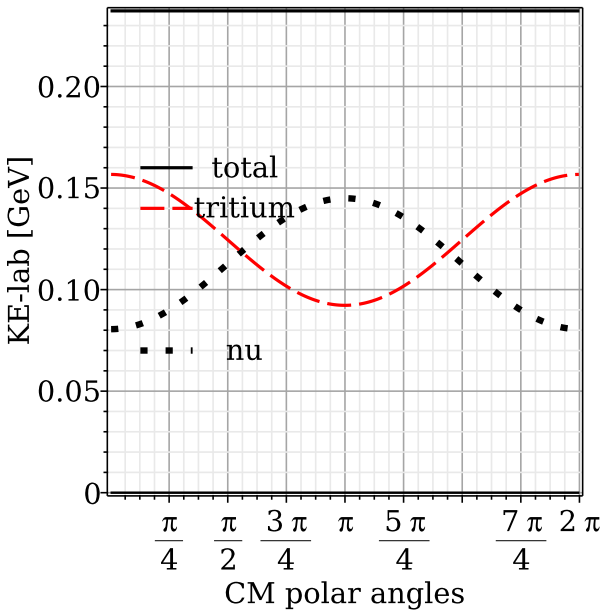

Figure 18. Plot of final state kinetic energies vs CM polar angles, for the $e^- + 3\text{He} \rightarrow \text{triton} + \nu$.

Table 6. Field strengths, kinematic data, and spin tunes for the initial state of the reaction $e^- + h \rightarrow t + \nu$.

bm 1	m1 GeV	G1	q1	beta1	Qs1	KE1 MeV	E0 MV/m	etaM	m2 GeV	G2	q2	beta2	KE2 MeV	Qs2	bratio	bm 2
h	2.8084	−4.1834	2	0.250 00	-8.641×10^{-1}	92.1000	9.2400	−0.1214	0.0005	0.0012	−1	0.999 99	145.1413	0.324 35	16.000 13	e

Table 7. Field strengths, kinematic data, and spin tunes for the reaction $e^- + h \longrightarrow t + \nu$.

bm 1	beta1	Qs1	KE1 MeV	E0 MV/m	etaM	beta2	Qs2	KE2 MeV	beta*	gamma*	M* GeV	Q12* MeV	4*bratio	bm 2
h	0.2500	−0.864	92.09	9.238	−0.121 38	1.00	0.324	145.12	0.285	1.043	2.919	110.120	0.999 94	e
h	0.2500	−0.864	92.10	9.240	−0.121 39	1.00	0.324	145.14	0.285	1.043	2.919	110.131	0.999 99	e
h	0.2500	−0.864	92.11	9.241	−0.121 40	1.00	0.324	145.15	0.285	1.043	2.919	110.142	1.000 04	e

Table 8. Field strengths, kinematic data, and spin tunes for the final state of the reaction $e^- + h \longrightarrow t + \nu$.

bm 3	m3 GeV	G3	q3	th3-90	th4-90	KE3 MeV	E0 MV/m	etaM	KE4 MeV	m4	G4	q4	bm 4
t	2.8089	7.9150	1	10.97	86.32	124.48	9.2400	−0.1214	112.7400	0.0000	0.0000	0	ν

Table 8 shows final state kinematic parameters for "electron induced triton β-reincarnation".

9.1 The importance of unitarity

Table 2 showed two examples of simultaneously-stored triton and helion beams. For helion kinetic energies roughly twice as great as tritium energies these isotopes can co- or contra-circulate compatibly — with velocities related by an integer ratio as desired.

Here we contemplate the possibility of electrons and helions co-circulating with velocities that are in integer ratio, in spite of their opposite signs. As before, the purpose is to reduce the e^- and h CM kinetic energies so as to enable rear-end collisions in a moving frame of reference.

Now, however, since there is no Coulomb barrier to overcome, the motivation is different. In this case the Coulomb force is attractive. Presumably, this is helpful for the collision cross section. It may also relax the ring space charge acceptance limitation.

A strong motivation for enabling rear-end collisions is to influence the detectable weak interaction rate by suppressing competing inelastic channels other than electron capture (EC).

This may seem to be counter-productive. As well as being very small, neutrino cross sections are proportional to the laboratory neutrino energy. Zuber's "Neutrino Physics" book, [32] provides total neutrino cross sections;

$$\begin{aligned} \sigma(\nu N) &= (0.677 \pm 0.014) \times 10^{-38}\,\mathrm{cm}^2 \times E_\nu/(\mathrm{GeV}) \\ \sigma(\bar{\nu} N) &= (0.334 \pm 0.008) \times 10^{-38}\,\mathrm{cm}^2 \times E_\nu/(\mathrm{GeV}) \end{aligned} \tag{9.1}$$

where N stands for p or n or their average.

Surely one wants the neutrino energies to be as large as possible, consistent with the maximum achievable electric field (which is inversely proportional to the ring bending radius)?

This reasoning is fallacious, however. During the compound nucleus phase of nuclear collisions there is a competition (to escape) amongst the various possible final state exit channels. By unitarity, only one of the possible exit channels can be responsible for any given detectable event. In this competition, low probability channels are strongly disadvantaged.

The only situation in which (low probability) electron capture has an advantage is when most or all other (high probability) inelastic channels are forbidden by energy conservation. This condition can be met for weak interactions by enabling only rear-end collisions in the $e^- + h \longrightarrow t + \nu$ channel, for which competing channels are forbidden by energy conservation.

2024 JINST 19 P11017

As with predominantly magnetic rings, head-on collisions would have large CM energies which would enable large cross section inelastic collisions which will suppress weak scattering elastic channels of lower energy. In other words "for CM energy, higher is not always better".

Nowadays one rarely hears accelerators referred to as "atom smashers", a term that was once in common usage in spite of always being somewhat misleading. The term "nucleus smasher" has never caught on, even though, at multi-GeV levels it would be quite apt. What is being proposed here could then be called a "nucleus tickler".

9.2 Unambiguous event reconstruction

Consider the channel $e^- + h \rightarrow t + \nu$, concentrating in particular on the unambiguous reconstruction of a foreground event such as illustrated in figure 20, which is a blow-up of the central part of figure 19. With the quadrupoles removed from alternating straight sections, one of the four free straight sections can be instrumented with annular tracking/polarimiter chambers with graphite film plates. A candidate triton trajectory begins, on axis at point (1), somewhere along the bunch overlap region. Its subsequent history can be reconstructed sequentially.

1. The initial scattering point is known to be a longitudinally centered point close to a fixed, but adjustable, intersection point (IP).

2. With the chamber azimuthally symmetric, the entry point (2) can be measured with high precision.

3. Within one of the graphite chamber (actually construction grade graphene) a triton-carbon nuclear scatters elastically at point (3) (with efficiency, i.e. probability, of say 1/500, from a carbon nucleus in one of the chamber plates. See appendix-B of [3]. Such a scatter measures the triton polarization with high analyzing power, greater than, say, 0.4.

4. The triton ranges out at point 4. The full 2,3,4 range is necessarily bounded (precisely, from above) by the stopping power of tritons in graphite.

This sequence of events provides unambiguous confirmation of the process interpretation. Such events can be expected to be azimuthally symmetric around the longitudinal axis. Five hundred times this many events, similarly azimuthally symmetric, will be reasonably ascribed to the process $e^- + h \rightarrow t + \nu$; but no polarization information is available for these events, especially those that range out with almost maximum range, under the assumption they are tritons.

9.3 Triton extraction, tracking, and polarimetry

Figure 20 shows an expected $h + e^- \rightarrow t + \nu$ event, with the triton stopping in a tracking chamber. The angles of the scattered particles are taken from table 8. where they are listed as "th3-90" and "th4-90", representing particle "3" (t) and particle "4" (ν) radiated at 90° in the CM system. These are maximum angles in the laboratory, at the Jacobean peak of the rainbow pattern. The corresponding kinetic energies are given in the same table.

Far more significant than the scattered triton direction is their factor of two reduced charge, compared to the helions they replace. Much like electron stripping injection, one has charge reduction extraction, as shown in figure 20.

2024 JINST 19 P11017

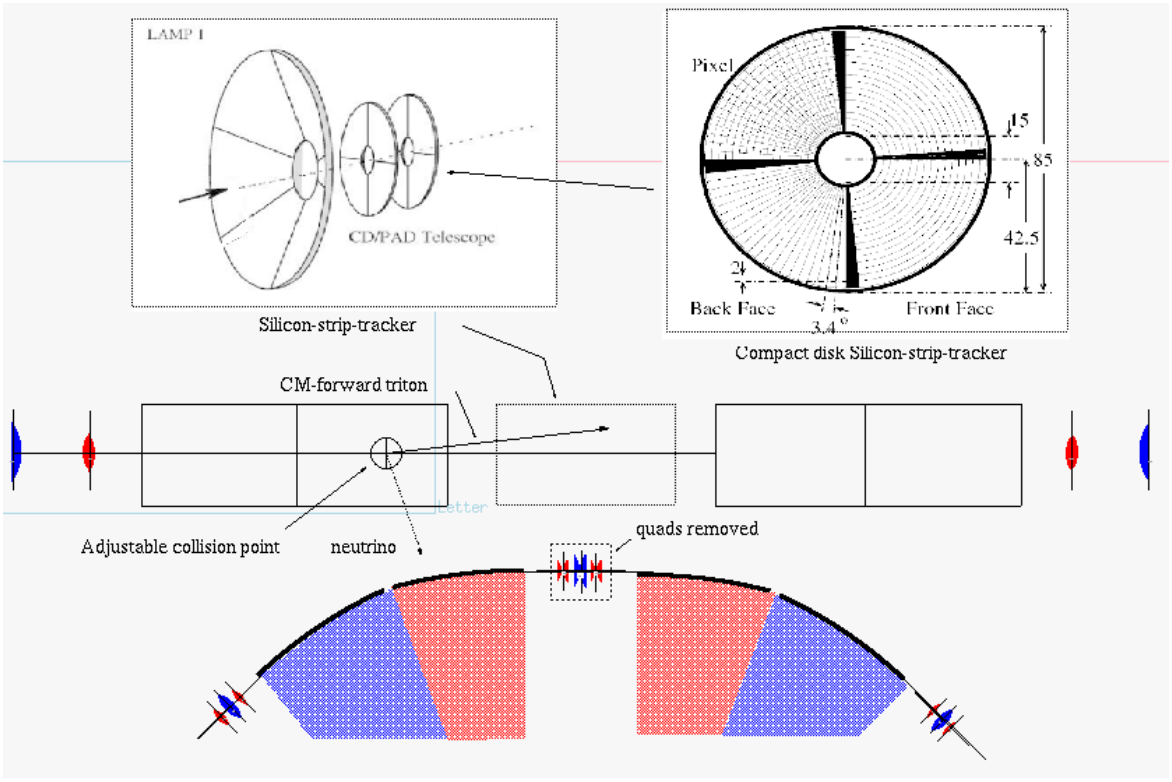

Figure 19. . An expected $h + e^- \rightarrow t + \nu$ event, with the triton stopping in a conceptual tracking chamber. The inset figures are reprinted from [33], Copyright (2002), with permission from Elsevier.

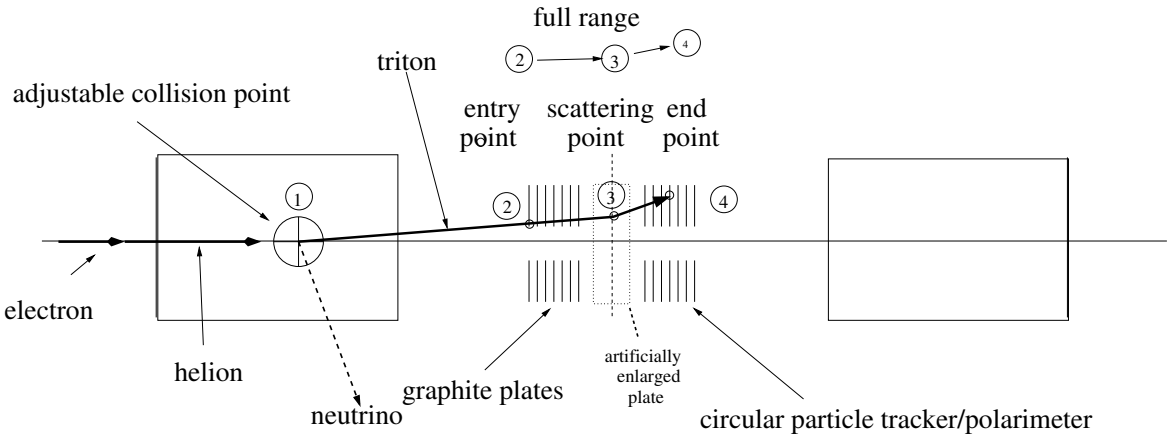

Figure 20. Figure showing alternative particle detection apparatus for recording an expected $h + e^- \rightarrow t + \nu$ event, with the triton stopping in the tracking chamber. The helion kinetic energy has been selected arbitrarily, though possibly higher in energy than could be handled in a ring with 11 m bending radius. Experimental considerations concerning practical experimental optimization have not been formulated.

2024 JINST 19 P11017

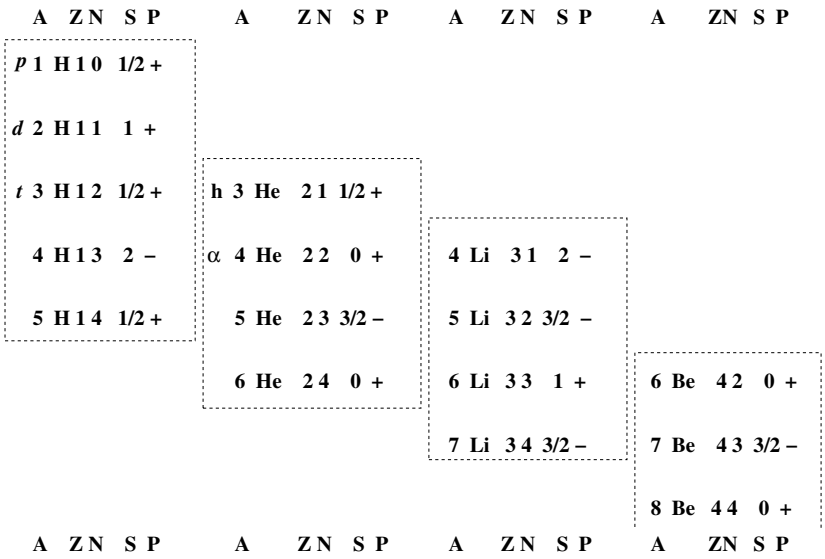

Figure 21. Figure showing (side-by-side) low mass ($0 < Z < 5,\ A < 9$) candidates for free electron or positron capture β-decay" transmutations. Every entry has at least a multi-year lifetime and can be linac-accelerated to 60 MeV/nucleon energy to produce mA-level average current beams with 1/2 percent energy spread [17].

At the cost of reducing the ring periodicity, the quadrupoles can be removed from half of the straight sections, in order to make room for both injection and extraction equipment. Injection is covered in some detail in reference [12].

Figure 21 shows practical low mass nuclear isotope transmutation possibilities. [17]

9.4 Weak interaction yearly rate

A worksheet calculation of the yearly EC event rate is displayed in figure 22. Neglecting beam shape variation bunching and injection, maintenance down-time, and other inconvenient details, a stripped down rate estimate with optimistic parameters follows; with $A = 3$, nucleon mass $M = 1$ GeV, electron energy $\mathcal{E}_e = 0.1$ GeV, ring circumference 100 m; radius of curvature $r_0 = 11$ m.

10 Recapitulation and conclusions

From the perspective of the present authors this paper represents the culmination of one sub branch of an experimental program to study time reversal invariance initiated by Norman Ramsey and Robert Purcell in 1957, with measurement of the neutron EDM being their first target. This program has continued ever since, most recently reducing the current neutron EDM upper limit to [34]; $d_n = (0.0 \pm 1.1_{\text{stat}} \pm 0.2_{\text{sys}} \times 10^{-26})\, e$ cm.

In a 2004 paper by Farley et al. [35], it was suggested that the muon EDM could be measured by freezing the muon spins (i.e. Q_s=0) of counter-circulating muons. By 2011 a plan for measuring the proton EDM in the all-electric 232 MeV storage ring (referred to previously in this paper as the "Nominal All-Electric Proton EDM ring") had been developed.

Shortly after this, a CPEDM Group was formed, led, initially, by BNL and by the COSY lab in Juelich, Germany, with participation more or less balanced between European (including Russian) and North American physicists, with co-leaders from the lead laboratories.

2024 JINST 19 P11017

$$
\begin{aligned}
\text{storage ring revolution frequency: } f_{\text{sr}} &= 3 \times 10^{6}\,\text{Hz},\\
\text{Fermi constant: } G_F &= 1.166 \times 10^{-5}\,\text{GeV}^{-2},\\
\text{Mandelstam CM-energy-squared. } 2\mathcal{E}_e A\, M\text{: } s &= 0.6\,\text{GeV}^2,\\
\text{total e,h Fermi cross section, } G_F^2 s/\pi \text{ : } \sigma_{\text{eh}} &= 2.60 \times 10^{-11}\,\text{GeV}^{-2},\\
\text{total e,h Fermi cross section: } \sigma_{\text{eh}} &= G_F^2 s/\pi\\
&= 2.60 \times 10^{-11}\,\text{GeV}^{-4},\\
\text{area unit conversion factor: } 1\,\text{GeV}^{-2} &= 0.329\,\text{mb},\\
\text{total e,h Fermi cross section in barn units: } \sigma_{\text{ht}} &= 2.81 \times 10^{-12}\,\text{mb}\\
\text{stored particles in each beam: } N_b &= 10^{12},\\
\text{beam area: } A_b &= 10^{-2}\,\text{cm}^2,\\
\text{full ring opacity (scattering fraction) } N_b\sigma_{\text{eh}}/A_h \text{ : } O_T &= 0.281 \times 10^{-22}\\
\text{full ring electron scattering rate } f_{\text{sr}} N_b O_T\text{: } rate_s &= 0.84 \times 10^{-4}/\text{second}\\
\text{tritium reincarnations per year } rate[s] \times 3 \times 10^7\text{: } rate[y] &= 2500/\text{year}
\end{aligned}
$$

Figure 22. Figure displaying a worksheet calculation, based on the original Fermi weak iteraction scattering rate formula, [24], for the yearly EC event rate for the process $h + e^- \rightarrow t + \nu$.

By 2018, however, for reasons best forgotten, having to do with program priorities, the CPEDM group had split, largely, but not entirely, into an American and a European proton EDM group. Nevertheless the work of the CPEDM group (including significant previous contributions from the American contingent) but authored by the European contingent, was documented in the CERN Yellow Report [12] referenced frequently in this paper.

The combination of COVID-19 and the CPEDM group schism naturally slowed progress on the proton EDM project. But it also led to the development by the "sub-branch" mentioned in the first sentence of this section — especially in the form of reference [14], in which the concept of small and inexpensive predominantly electric E&m storage rings were proposed in which "doubly magic" protons and helions (i.e. both spin tunes zero) could counter-circulate simultaneously, thereby enabling measurement of the difference of proton and helion EDM's (which are expected to vanish individually, by time reversal) could be measured. Since the dominant systematic error cancels in this difference, this test of T-violation is more sensitive than either EDM measurement could be individually.

The same paper also showed that both spin tunes in the nominal all-electric proton EDM ring could not be globally frozen without the intentional inclusion of some magnetic bending. Furthermore, with minimally strong magnetic field (to freeze both beam spin tunes) the spin tune difference would be inconveniently small. Overcoming this problem would lead more nearly to the configuration described in the present paper.

Significant as it was, this particular proton minus helion EDM measurement development cannot be said to make the EDM measurement easy. *What follows in the present paper is easy*, at least by comparison.

It soon became apparent that, as well as enabling counter-circulation, E&m bending would also enable co-circulation of various particle types. This led to the rear-end collisions and the capability of controlling the initial-state spins and measuring the final state spins which constitutes the main

2024 JINST 19 P11017

body of the present paper. Unlike the EDM measurement, these low energy nuclear measurements seem to be not very challenging to perform experimentally. Subsequently, an especially promising weak interaction β-decay channel, namely $e^- + h \rightarrow t + \nu$, suggested itself.

Based on the numerous low energy nuclear channels analyzed in this paper, *what is being proposed is an inexpensive, yet powerful, low energy nuclear physics program, rather than any individual project*. The program can be expected to include investigation of the spin dependence of nuclear scattering and transmutation, including weak nuclear interactions.

The goals therefore are to provide experimental data sufficient to refine our understanding of the nuclear force (to the extent it can be disentangled from the electromagnetic force) and nuclear physics.

Pure incident spin states, high analyzing power final state polarization measurement, and high data rates should initiate a qualitatively and quantitatively new level of experimental observation of nuclear reactions.

Especially important is the investigation of wave particle duality and spin dependence of "elastic" p, d scattering below the pion production threshold. Precision comparison of "light on heavy" and "heavy on light" collisions (which would be identical for point particles, but not necessarily for compound particles) can also probe the internal nuclear structure; perhaps distinguishing experimentally between "prompt" and "compound nucleus" scattering. This promises to provide a more instructive visualization of internal structure than can be produced by the parton picture obtained by ultra-high momentum transfer inelastic electron scattering.

This paper has described an E&m storage ring capable of the room temperature laboratory spin control of two particle nuclear scattering or fusion events. The novel equipment making this possible is a storage ring with superimposed electrical and magnetic bending. Rings like this were introduced by Koop but have not yet been built.

Serving as a demonstration of nuclear to electrical energy conversion, such apparatus can perform measurements needed to refine our understanding of thermonuclear power generation and cosmological nuclear physics. It is the novel capability of such rings to induce "rear-end" nuclear collisions that makes this possible.

Emphasizing the measurement of spin dependence in low-energy nuclear physics, the goal is to provide experimental data to refine our understanding of nucleon composition along with the nuclear force and its influence on elementary-particle physics. The better understanding of low energy nuclear processes that can be obtained from the proposed improvement of experimental measurement methods seems certain to enhance cosmological nuclear physics.

Ironically, this improvement will have been produced by the use of storage rings to investigate nuclear processes at the *reduced kinetic energies of cosmological nuclear physics*, compared to presently available fixed target measurements.

References

[1] R. Talman, *Prospects for Electric Dipole Moment Measurement Using Electrostatic Accelerators*, *Rev. Accel. Sci. Tech.* **10** (2019) 267.

[2] R.M. Talman, *Superimposed electric/magnetic "dipole moment comparator" lattice design*, 2021 *JINST* **16** P09006 [arXiv:2108.12353].

[3] R. Talman and J. Talman, *Predominantly electric storage ring with nuclear spin control capability*, arXiv:2402.04109.

2024 JINST 19 P11017

[4] National Bureau of Standards Physical Measurement Laboratory, https://physics.nist.gov.

[5] Background information related to the constants, https://physics.nist.gov/cuu/Constants/background.html.

[6] Atomic Weights and Isotopic Compositions for All Elements, https://physics.nist.gov/cgi-bin/Compositions/stand_alone.pl.

[7] R.M. Talman, *Superimposed electric/magnetic "dipole moment comparator" lattice design*, 2021 *JINST* **16** P09006 [arXiv:2108.12353].

[8] A. Jaffe, *Quantum Theory and Relativity*, George Mackey celebration, Harvard University (2007).

[9] M. Pavsic, *External inversion, internal inversion, and reflection invariance*, *Int. J. Theor. Phys.* **9** (1974) 229 [hep-ph/0105344].

[10] I. Koop, *Asymmetric Energy Colliding Ion Beams in the EDM Storage Ring*, in the proceedings of the *4th International Particle Accelerator Conference*, Shanghai, China, 12–17 May 2013, pp. 1961–1963, https://jacow.org/IPAC2013/papers/TUPWO040.pdf.

[11] R. Talman, *The Electric Dipole Moment Challenge*, IOP Publishing (2017) [DOI:10.1088/978-1-6817-4509-1].

[12] CPEDM collaboration, *Storage ring to search for electricdipole moments of charged particles: Feasibility study*, CERN, Geneva (2021) [DOI:10.23731/CYRM-2021-003].

[13] https://github.com/jtalman/ual1/tree/master/examples/lattices.

[14] R.M. Talman, *Difference of measured proton and He3 EDMs: a reduced systematics test of T-reversal invariance*, 2022 *JINST* **17** P11039 [arXiv:2205.10526].

[15] J. Haissinski, *The Orsay Electron-Positron Storage Ring (Status Report)*, *Conf. Proc. C* **6906161** (1969) 141.

[16] J. Boeker, K. Grigoriev et al., *Work program for the development of electrostatic deflector elements for storage rings*, Internal IKP report, Jülich, Germany (2020).

[17] Private communication with Deepak Raparia, BNL Collider Accelerator Department (2024).

[18] R. Albrecht, *Das Potential in doppelt gekrümmten Kondensatoren*, *Z. Naturforsch. A* **11** (1956) 156.

[19] M. Plotkin, *The Brookhaven electron analogue, 1953–1957*, BNL Report 45058, Brookhaven, NY, U.S.A. (1991).

[20] R.M. Talman and J.D. Talman, *Symplectic orbit and spin tracking code for all-electric storage rings*, *Phys. Rev. ST Accel. Beams* **18** (2015) 074003 [arXiv:1503.08468].

[21] C. Wilkin, *The legacy of the experimental hadron physics programme at COSY*, *Eur. Phys. J. A* **53** (2017) 114 [arXiv:1611.07250].

[22] P. Lenisa et al., *Low-energy spin-physics experiments with polarized beams and targets at the COSY storage ring*, *EPJ Tech. Instrum.* **6** (2019) 2.

[23] H.C. van-de-Hulst *Light Scattering by Small Particles,* Dover Publications (1981) [originally, John Wiley and Sons, Inc., NY, U.S.A. (1957)]

[24] E. Fermi, *High Energy Nuclear Events*, *Prog. Theor. Phys.* **5** (1950) 570.

[25] R. Hagedorn, *Relativistic kinematics: a guide to the kinematic problems of high-energy physics*, W.A. Benjamin Inc., New York, NY, U.S.A. (1960).

[26] JEDI collaboration, *New method for a continuous determination of the spin tune in storage rings and implications for precision experiments*, *Phys. Rev. Lett.* **115** (2015) 094801 [arXiv:1504.00635].

2024 JINST 19 P11017

[27] JEDI collaboration, *Phase locking the spin precession in a storage ring*, *Phys. Rev. Lett.* **119** (2017) 014801 [arXiv:1703.07561].

[28] F. Rathmann, N.N. Nikolaev and J. Slim, *Spin dynamics investigations for the electric dipole moment experiment*, *Phys. Rev. Accel. Beams* **23** (2020) 024601 [arXiv:1908.00350].

[29] JEDI collaboration, *First detection of collective oscillations of a stored deuteron beam with an amplitude close to the quantum limit*, *Phys. Rev. Accel. Beams* **24** (2021) 124601 [arXiv:2101.07582].

[30] F. Rathmann, *First Direct Hadron EDM Measurement With Deuterons Using COSY*, in *Willy Haeberli Memorial Symposium* (2022), https://www.physics.wisc.edu/haeberli-symposium/.

[31] A. Zelenski et al., *Optically pumped polarized $^3He^{++}$ ion source development for RHIC/EIC*, *Nucl. Instrum. Meth. A* **1055** (2023) 168494 [arXiv:2303.10409].

[32] K. Zuber, *Neutrino Physics*, CRC Press, Taylor & Francis Group, Boca Raton (2012) [DOI:10.1201/9781315195612].

[33] A.N. Ostrowski et al., *CD: A double sided silicon strip detector for radioactive nuclear beam experiments*, *Nucl. Instrum. Meth. A* **480** (2002) 448.

[34] C. Abel et al., *Measurement of the Permanent Electric Dipole Moment of the Neutron*, *Phys. Rev. Lett.* **124** (2020) 081803 [arXiv:2001.11966].

[35] F.J.M. Farley et al., *A new method of measuring electric dipole moments in storage rings*, *Phys. Rev. Lett.* **93** (2004) 052001 [hep-ex/0307006].

[36] E.W. Otten and C. Weinheimer, *Neutrino mass limit from tritium β decay*, *Rept. Prog. Phys.* **71** (2008) 086201 [arXiv:0909.2104].

2024 JINST 19 P11017